Complex zoning and resorption of phenocrysts in mixed potassic mafic magmas of the Highwood Mountains, Montana

Hugh E. O'Brien,* Anthony J. Irving, I. Stewart McCallum

Department of Geological Sciences, University of Washington, Seattle, Washington 98195, U.S.A.

Abstract

Disequilibrium phenocryst assemblages and complex compositional zoning in clinopyroxene, mica, and olivine phenocrysts provide a detailed record of multiple mixing, fractional crystallization, and degassing events during the high-level evolution of potassic mafic magmas in the Eocene Highwood Mountains province. The contrasting phenocryst assemblages of minettes (diopside + phlogopite ± olivine) and mafic phonolites–shonkinites (salite + leucite ± olivine) permit unambiguous documentation of mixing between these two magma types and also between more primitive and more evolved members of each type.

The varied behavior of crystals mixed into disequilibrium liquids, deduced from detailed textural and microprobe analyses, is consistent with the results of experimental studies of plagioclase dissolution. Phlogopite and diopside xenocrysts within more evolved mafic phonolite liquids initially underwent peripheral resorption. Further dissolution of diopside produced a network of interior cavities that were subsequently plated by salite crystallized from the host magma. In contrast, salite xenocrysts within more primitive mafic phonolite liquids underwent partial dissolution at their margins, yet remained euhedral. In some cases dissolution was restricted to a single, compositionally distinct sector. Halos of Fe-Al–rich salite subsequently formed around the melt-filled cavities by diffusion.

Complexly zoned salite and biotite crystals containing one or more sharply bounded, epitaxial bands of diopside and phlogopite, respectively, are common in the mafic phonolites and shonkinites. On the basis of features such as the different salite compositions on either side of diopside bands and their lack of leucite inclusions and oscillatory zoning, it is argued that each band in a crystal (rarely more than six) is a record of a mixing event with minette magma.

We infer that the contrasting phenocryst assemblages of the compositionally similar minettes and mafic phonolites largely reflect differences in H_2O activity during their crystallization, and we propose that degassing of ascending minette magmas was an important petrogenetic process. We conclude that the high-level evolution of the Highwood magmatic system involved repeated mixing in multiple reservoirs among batches of variably fractionated and degassed mafic phonolite magma and periodic influxes of more primitive, undegassed minette magma.

Introduction

Magma mixing has become increasingly recognized as an important process in the evolution of many magmatic systems. Hybrid magmas may form by mixing of magmas derived from different sources or by mixing of magmas from a common source but at different stages on a liquid line-of-descent. Evidence commonly cited for mixing includes textural and chemical disequilibrium in phenocryst assemblages (e.g., Brooks and Printzlau, 1978; Gerlach and Grove, 1982), variability of melt inclusion compositions (e.g., Dungan and Rhodes, 1978), linear trends of major- and trace-element variation diagrams (e.g., Langmuir et al., 1978), reversals of predicted crystallization sequences for basalts (e.g., Walker et al., 1979) and for cumulate sequences (e.g., Raedeke and McCallum, 1984), and variations in isotopic ratios (e.g., Dungan et al., 1986).

In this paper, we present integrated textural and mineral-chemical evidence for magma mixing in the potassic mafic volcanic and intrusive rocks of the Highwood Mountains, Montana. The marked mineralogical contrast between minette and mafic phonolite magmas in this

---

* Present address: Geological Survey of Finland, SF-02150 Espoo 15, Finland.
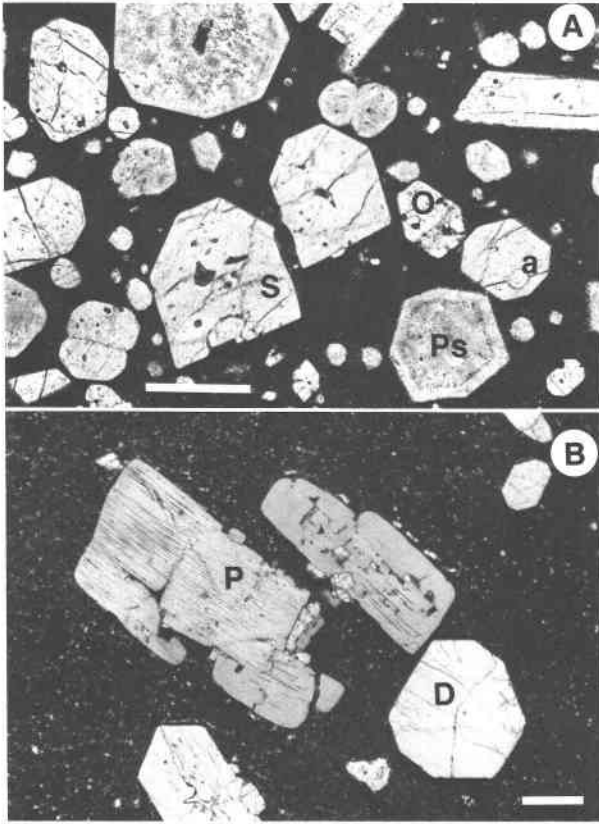
Fig. 1. Photomicrographs of typical mafic phonolite and intermediate minette dike samples from the Highwood Mountains province. (A) The seriate porphyritic mafic phonolite (HM-144) contains phenocrysts of pseudoleucite [Ps], salite [S], and olivine [O] in a groundmass composed mostly of sanidine and microphenocrysts of salite and biotite; [a] = apatite inclusion in salite. (B) The hiatal porphyritic minette (HM-552) contains phenocrysts of phlogopite [P] and diopside [D] in a fine-grained, sanidine-rich groundmass. Plane-polarized light; scale bar is 0.5 mm.

province allows unambiguous documentation of the nature and extent of mixing and, additionally, has led to the recognition of degassing as an important petrogenetic process. Clinopyroxene, mica, and olivine phenocrysts have preserved a remarkably detailed record of multiple mixing, fractional crystallization, and degassing events. We conclude that, during the high-level evolution of the Highwood magmatic system, batches of variably fractionated and degassed mafic phonolite magma in near-surface reservoirs were periodically mixed with each other and with influxes of more primitive, undegassed minette magma. We believe that such a model has important implications for other alkalic magmatic systems.

GEOLOGIC SETTING

The north-central Montana alkalic province consists of several centers of potassic mafic volcanism containing rock types ranging from mafic phonolites, minettes, and lamproites to alnoites, monticellite peridotites, and kimberlites (Larsen, 1940; Hearn, 1979; Marvin et al., 1980). Located 50 km east of Great Falls, the Highwood Mountains represent a deeply incised, 53–50 Ma volcanic edifice (Marvin et al., 1980), the remnant of which is now roughly 30×20 km. An early sequence of quartz-normative latite breccias, flows, and tuffs is overlain by SiO_2-undersaturated potassic mafic volcanics. Mafic phonolite flows and flow breccias constitute 80% of the latter with mafic phonolite lahar deposits and tuffs composing the remainder. Minette flows are rare, and only one minette tuff has been found. The intrusion of shonkinite and syenite stocks, up to 5 km across, into the volcanic pile caused doming and disruption of the volcanic stratigraphy by high-angle normal and reverse faulting. Mafic phonolite, minette, and syenite dikes from 10 cm to 5 m in width crosscut both the volcanics and the stocks. The volumes of minette and mafic phonolite dikes are roughly equal, in sharp contrast to the rarity of extrusive minettes. Areas where the country rock has been completely displaced by dike swarms (continuous dike on dike contacts) reach up to 0.5 km in width.

ROCK TYPES

The Highwood Mountains is the type locality for shonkinite and several much rarer rock types (e.g., missourite and fergusite—Weed and Pirsson, 1895; Pirsson, 1905). However, only the major rock types of the younger suite (mafic phonolite, shonkinite, and minette) will be discussed in this paper. For a complete survey the reader is referred to the classical work of Pirsson (1905) and Larsen et al. (1941).

The minettes, mafic phonolites, and shonkinites have virtually identical ranges in bulk chemical composition despite having different mineral assemblages. The striking difference between minettes with abundant phlogopite and mafic phonolites rich in leucite (Fig. 1) must reflect differences in H_2O activity during crystallization. Similar bimodal hydrous and anhydrous suites have been described from the K-rich rocks of the Muriah Complex, Java (Nicholls and Whitford, 1983) and from the Navajo Field, southwest U.S.A. (Williams, 1936). We have suggested that this bimodality in the Highwood province is the result of degassing of parental minette magma at high levels within the magma system (O'Brien et al., 1986).

Mafic phonolite

These seriate porphyritic rocks contain between 20% and 60% phenocrysts of olivine, salite, and pseudomorphs of leucite in a fine-grained groundmass of sanidine, pseudoleucite, salite, biotite, apatite, and titanomagnetite (Fig. 1A). On the basis of phenocryst mineralogy, the majority of the Highwood leucite-phyric flows and dikes would be more correctly termed "olivine
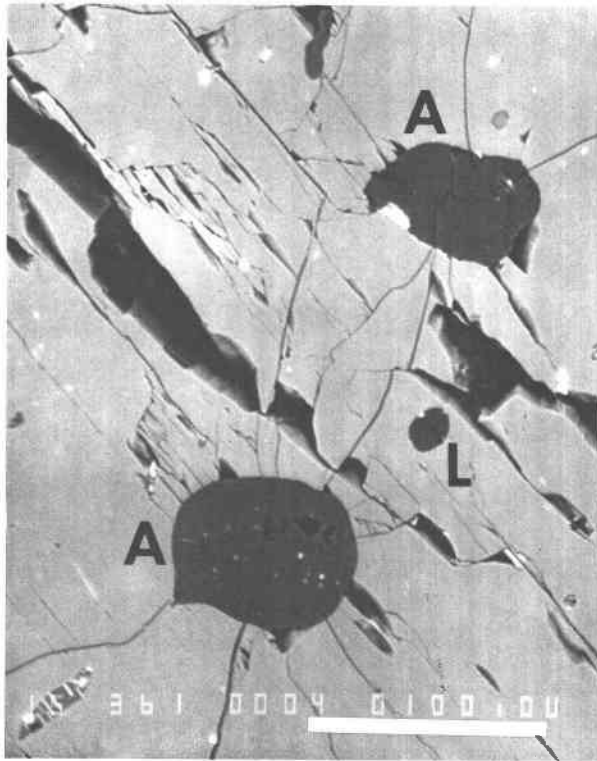
Fig. 2. Inclusions of fresh leucite [L] and analcimized leucite [A] within a salite phenocryst from a mafic phonolite. Radial fractures in the host salite around the two analcimized leucite inclusions are interpreted to have resulted from expansion during hydration. Backscattered-electron image; scale bar is 100 μm.

TABLE 1. Leucite and analcime compositions

	Leucite			Analcime			
	Incl.	Incl.	Incl.	Incl.	Incl.	Cav.	Phen.
SiO$_2$	56.4	55.6	56.2	54.4	54.4	54.8	54.8
Al$_2$O$_3$	22.7	22.8	22.6	22.5	22.4	22.1	22.0
CaO	0.15	0.31	0.25	0.51	0.07	0.35	0.04
Na$_2$O	0.99	0.55	0.55	11.8	12.6	11.6	12.3
K$_2$O	20.0	20.4	20.3	0.47	0.50	0.68	0.89
BaO	b.d.	0.23	0.24	0.02	b.d.	b.d.	0.08
Total	100.21	99.82	100.22	89.68	89.94	89.53	90.09
	Cations based on six oxygens						
Si	2.028	2.016	2.030	2.029	2.029	2.045	2.041
Al	0.963	0.974	0.960	0.988	0.982	0.973	0.968
Ca	0.006	0.012	0.003	0.020	0.003	0.014	0.002
Na	0.069	0.039	0.039	0.856	0.909	0.841	0.886
K	0.919	0.944	0.935	0.022	0.024	0.032	0.042
Ba	0.000	0.003	0.003	0.001	0.000	0.000	0.001
Total	3.985	3.988	3.970	3.916	3.947	3.905	3.940

Note: Incl. = inclusion in salite, Cav. = analcime inside of groundmass-filled cavity in salite, Phen. = analcimized leucite phenocryst, b.d. = below detection limits. Analytical conditions for all microprobe data: 15-kV acceleration potential, 5- to 30-nA sample current. Standards included natural hyalophane, orthoclase, albite, biotite, forsterite, clinopyroxene, and synthetic diopside-jadeite glass and fluorphlogopite. Data were corrected using a Bence-Albee correction procedure (Bence and Albee, 1968).

leucitites" (80%) and "leucitites" (15%), using the classification scheme of Streckeisen (1979). Sanidine-phyric samples (5% of the total) are, however, correctly termed "phonolite." Apparently, the abundance of groundmass sanidine and the presence of hyalophane phenocrysts in some of the more evolved samples compelled Larsen et al. (1941) to classify all of these rocks as members of the phonolite clan. Even though the term "mafic phonolite" is somewhat misleading, we have continued its usage because it is entrenched in the literature.

Salite phenocrysts commonly exhibit well-developed oscillatory and sector zoning. Adjacent sectors (e.g., [001] zone sectors relative to ($\bar{1}$11) sectors) exhibit compositional differences that are greater than the variations due to normal zoning within each sector. Oscillatory zoning is emphasized by parallel growth layers containing abundant inclusions of apatite, leucite, titanomagnetite, and glass ($\pm$ fluid).

Olivine ranges from Fo$_{84}$ in the most primitive mafic phonolites to Fo$_{45}$ in the more evolved varieties. The most prevalent olivine compositions are Fo$_{77}$ to Fo$_{80}$.

Occurrences of fresh leucite phenocrysts are rare in the mafic phonolites. Most commonly, phenocrysts that macroscopically appear to be leucite consist of either pseudoleucite (a fine-grained, spherulitic intergrowth of nepheline and sanidine) or analcime (ranging from turbid brown to perfectly clear). However, salite and olivine phenocrysts commonly contain abundant, pristine leucite inclusions up to 50 μm across. Inclusions of analcime are also present, but they are associated with cracks in the host crystal and are surrounded by radiating fractures (Fig. 2). We interpret these to be completely analcimized leucite grains that have undergone expansion during hydration. Table 1 gives analyses of representative fresh leucite inclusions, analcimized leucite inclusions, and an analcime "phenocryst." The following observations suggest that all of the Highwood Mountains analcime "phenocrysts" are secondary: (1) analcime inclusions in salites are always associated with cracks in the host crystals; (2) the analcimization of leucite inclusions was always complete; (3) leucite inclusions occur in salites from all analcime "phenocryst"-bearing samples, yet experimental studies (e.g., Fudali, 1963; Taylor and MacKenzie, 1975; Roux and Hamilton, 1976) show that analcime and leucite cannot stably coexist. Furthermore, even though pseudoleucite is abundant in many samples, no Na-rich leucite inclusions have been found. This is not consistent with the formation of pseudoleucite by the subsolidus breakdown of magmatic Na-rich leucite, a process suggested by Fudali (1963) and Watkinson (1973).

Many of the mafic phonolites contain xenocrysts of phlogopite and diopside. Phlogopite xenocrysts are subhedral to rounded, have biotite reaction rims, and commonly contain diopside inclusions. Diopside occurs as discrete xenocrysts, as cores to salite crystals, and as continuous growth bands within salite crystals.

TABLE 2. Mica compositions

	1	2	3	4	5	6	7	8	9	10
SiO$_2$	40.13	33.38	34.56	38.88	33.73	33.09	36.03	40.25	38.34	40.31
TiO$_2$	1.09	4.14	5.76	0.74	5.05	5.34	3.15	1.06	2.35	0.99
Al$_2$O$_3$	14.12	14.41	15.33	14.09	14.67	14.39	14.77	14.01	14.95	13.95
Cr$_2$O$_3$	1.01	b.d.	b.d.	1.27	b.d.	b.d.	b.d.	0.59	0.05	0.74
FeO	4.51	12.99	13.34	4.51	11.75	10.39	11.44	5.24	7.85	5.57
MnO	0.07	0.19	0.18	0.03	0.17	0.12	0.08	0.06	0.10	0.07
MgO	23.36	15.28	14.28	24.09	16.04	17.18	17.90	23.47	20.83	22.96
CaO	0.07	0.16	0.06	0.09	0.13	0.17	0.04	0.02	0.02	0.03
BaO	0.67	4.10	4.21	0.55	4.94	7.08	2.25	0.52	1.26	0.47
K$_2$O	9.85	8.02	8.15	10.24	8.21	7.79	8.71	10.03	9.46	10.10
Na$_2$O	0.08	0.57	0.52	0.25	0.56	0.40	0.20	0.13	0.19	0.12
F	0.52	1.59	1.40	0.28	1.04	0.99	0.97	0.96	0.91	0.92
	95.19	94.91	97.87	95.03	96.43	96.93	95.54	96.34	96.31	96.23
O=F	0.22	0.67	0.59	0.12	0.44	0.42	0.41	0.41	0.38	0.39
Total	94.97	94.24	97.28	94.91	95.99	96.51	95.13	95.93	95.93	95.84
					Cations based on 22 oxygens					
Si	5.755	5.256	5.247	5.624	5.199	5.114	5.433	5.760	5.581	5.782
Al	2.387	2.674	2.743	2.402	2.665	2.621	2.625	2.363	2.564	2.359
Ti	0.118	0.490	0.658	0.081	0.585	0.621	0.357	0.114	0.257	0.107
Cr	0.115	0.000	0.000	0.145	0.000	0.000	0.000	0.067	0.006	0.084
Fe	0.541	1.711	1.694	0.546	1.515	1.343	1.443	0.627	0.956	0.668
Mn	0.009	0.025	0.023	0.004	0.022	0.016	0.010	0.007	0.012	0.009
Mg	4.993	3.586	3.232	5.194	3.685	3.957	4.023	5.006	4.520	4.909
Ca	0.011	0.027	0.010	0.014	0.021	0.028	0.006	0.003	0.003	0.005
Ba	0.038	0.253	0.250	0.031	0.298	0.429	0.133	0.029	0.072	0.026
Na	0.022	0.174	0.153	0.070	0.167	0.120	0.058	0.036	0.054	0.033
K	1.802	1.611	1.579	1.890	1.614	1.536	1.675	1.831	1.757	1.848
Total	15.789	15.809	15.589	16.001	15.774	15.783	15.764	15.844	15.782	15.830

Note: Columns are (1) minette phlogopite phenocryst, (2) mafic phonolite biotite microphenocryst, (3) shonkinite biotite grain, (4) phlogopite xenocryst in mafic phonolite, (5) biotite rim on xenocryst in col. 4, (6) missourite biotite grain, and (7–10) complexly zoned mica (7 = biotite rim, 8 = phlogopite band, 9 = biotitic phlogopite band, 10 = phlogopite core); b.d. = below detection limits.
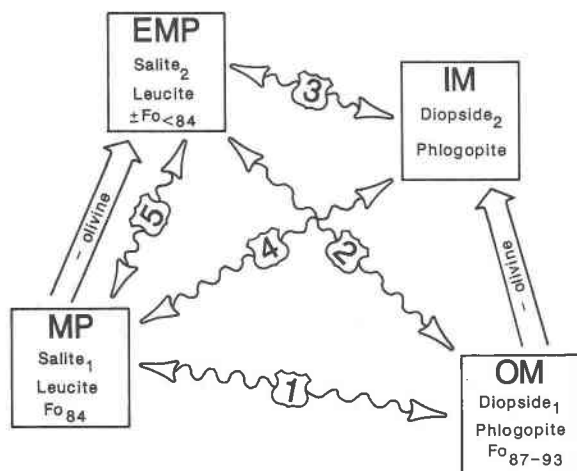
EMP = Evolved Mafic Phonolite
IM = Intermediate Minette
MP = Mafic Phonolite
OM = Olivine Minette

Fig. 3. Schematic diagram depicting the most common fractionation and mixing paths observed among magma types of the Highwood Mountains province and the phenocryst assemblages of each end member. The most primitive magma types at the bottom are linked by broad arrows to more evolved magma types at the top. These fractionation trends involve removal of olivine, clinopyroxene, and mica and result in compositional changes in mafic phenocryst phases (e.g., Mg/(Mg + Fe) of salite 2 < Mg/(Mg + Fe) of salite 1). Fractional crystallization beyond IM and EMP has yielded evolved minette and syenitic magmas, but these are not commonly observed as mixtures with the most primitive magma types. The five numbered wavy lines denote the mixed assemblages discussed in the text.

Shonkinite

This rock type is the equigranular, medium- to coarse-grained equivalent of mafic phonolite. Some of the larger mafic phonolite dikes and sills have porphyritic shonkinite cores, but by far the largest volume of shonkinite occurs in the five major stocks that have intruded the volcanic pile. Shonkinites have essentially the same mineral assemblage as mafic phonolites; however, slower cooling resulted in the following petrographic differences: (1) pseudoleucite occurs as coarse intergrowths of nepheline and sanidine rather than spherulitic intergrowths, and analcime is rare; (2) biotite forms large (up to 1 cm) subhedral, poikilitic crystals; (3) coarse sanidine and nepheline (the latter ~10% by volume) form an interstitial mosaic; (4) salite crystals do not have the narrow, fassaitic rims that are a common feature of salite phenocrysts in mafic phonolites; (5) only porphyritic shonkinites that are texturally gradational to mafic phonolites contain phlogopite xenocrysts (highly corroded); and (6) all diopside xenocrysts are enclosed within mantles of salite.

Minette

The most distinctive feature of these rocks is the abundance of large phlogopite phenocrysts (up to 2 cm across) that, along with diopside phenocrysts, are imbedded in a fine-grained matrix of sanidine, salite, biotite, titanomagnetite, and pyrite (Fig. 1B). Weed and Pirsson (1895) and Pirsson (1905) correctly identified this rock type as "minette," but Larsen et al. (1941) later redesignated it "biotite phonolite." Three minette subgroups can be distinguished: (1) olivine-bearing minettes, which, in addition
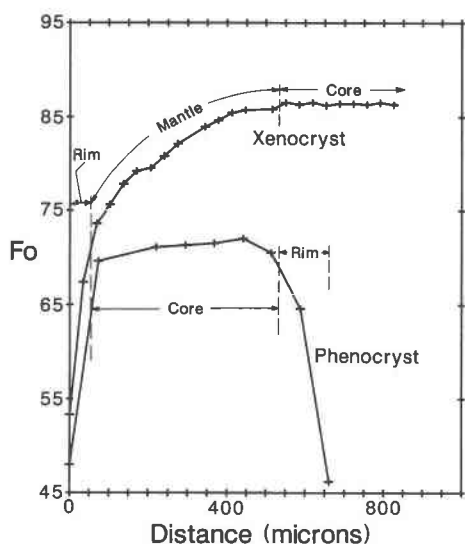
Fig. 4. Variation in Fo content across an olivine xenocryst and an olivine phenocryst from evolved mafic phonolite HM-107 (mixed assemblage 2). The mantle of the xenocryst is interpreted to result from continuous reaction with mafic phonolite magma toward a composition like that of equilibrium phenocryst cores. Note the similarity in size of the xenocryst reaction mantle and the phenocryst core. Both crystals have sharply defined, Fe-rich outer rims.

Fig. 5. Mica crystal from mixed mafic phonolite–minette HM-418a (mixed assemblage 4). A rounded xenocrystic core of phlogopite (dark gray) is in sharp contact with a more Fe-Ti–rich mantle. This is surrounded by an outer rim of biotite (light gray), which is similar to biotite in the groundmass. Backscattered-electron image; scale bar is 100 μm.

to phlogopite and diopside, contain forsteritic olivine phenocrysts, (2) intermediate minettes, which lack olivine and have a distinctive hiatal porphyritic texture, and (3) evolved minettes, with <10% phlogopite and salitic diopside in a sanidine-rich groundmass. Olivine phenocrysts in the most primitive minettes range from Fo_{94} (cores) to Fo_{87} (rims) and are compositionally distinct from the those in mafic phonolites (Fo_{84} to Fo_{45}).

Some of the intermediate and evolved minettes contain both diopside phenocrysts and large, discrete salite xenocrysts. These samples may also contain subhedral sanidine-rich globular structures that possibly represent reacted leucite xenocrysts, as suggested by Sheraton and England (1980) for similar features in lamproite dikes from Antarctica.

MIXED PHENOCRYST ASSEMBLAGES

Samples with mixed phenocryst assemblages are abundant in the Highwood province and are readily identifiable because the phenocrysts of the minettes and the mafic phonolites are so distinctive. Figure 3 schematically summarizes the five most common mixing paths between the four dominant end-member magma types. Assemblages 1 and 4 are commonly dominated by a mafic phonolite component, assemblage 2 by a minette component, and assemblage 3 can be dominated by either. Assemblage 5 has no minette component, but, rather, represents mixing between more evolved and more primitive mafic phonolites. Crystals of olivine, phlogopite, and clinopyroxene in these mixed assemblages show abundant evidence of disequilibrium with the mixed liquids.
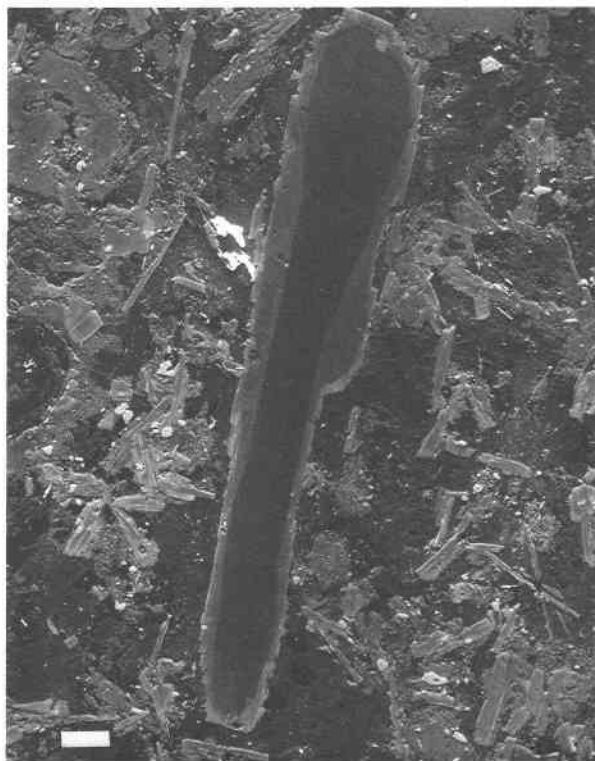
Olivine xenocrysts

Large subhedral xenocrysts of forsteritic olivine (Fo_{85} to Fo_{87}) up to 1 cm in width occur with diopside and phlogopite xenocrysts in some relatively evolved mafic phonolites. A core-to-rim zoning profile of a xenocryst from dike rock HM-107 (Fig. 4) shows a narrow (<40 μm) Fe-rich rim, a compositionally gradational mantle, and a uniform Mg-rich core ($Fo_{\sim 87}$). Also show in Figure 4 is a rim-to-rim profile of the largest olivine phenocryst in the same thin section. The outermost mantle composition of the xenocryst is approximately Fo_{71}, similar to that of the phenocryst core. The width of the xenocryst mantle is roughly the same as the width of the phenocryst core.

Zoning features similar to these have been described by Gerlach and Grove (1982) in reverse-zoned olivine crystals from Modoc basaltic andesites. Extending their interpretations, we suggest that the compositionally gradational mantles in the Highwood olivine xenocrysts may not represent simple normal zoning, but instead have resulted from diffusive re-equilibration subsequent to mixing. For the specific example described above, we infer that Fo_{71} olivine was plated onto the Fo_{87} xenocryst core for the same length of time as it took to grow the Fo_{71}

TABLE 3. Clinopyroxene compositions

No.:	Alpha				Beta			Gamma					
	1 core	2 band	3 mantle	4 rim	5 core	6 halo	7 mantle	8 core	9 mantle band 1	10 mantle band 2	11 mantle band 3	12 mantle band 4	13 mantle band 5
SiO_2	53.2	48.6	49.6	42.1	53.8	49.7	51.5	52.6	47.7	50.5	49.8	50.1	48.9
TiO_2	0.19	1.04	0.67	0.51	0.20	0.82	0.42	0.22	1.19	0.58	0.63	0.61	0.70
Al_2O_3	1.44	6.18	3.96	14.8	1.08	4.28	2.37	2.40	6.22	3.79	4.59	3.90	4.52
Cr_2O_3	0.42	0.09	0.40	0.09	0.27	0.09	0.06	0.14	0.04	0.30	0.20	0.26	0.05
FeO_{tot}*	3.46	7.82	6.40	19.2	3.16	7.47	8.09	4.79	8.37	6.47	7.07	6.45	7.66
MnO	0.10	0.17	0.13	0.92	0.15	0.20	0.36	0.14	0.21	0.16	0.19	0.16	0.18
MgO	17.2	12.8	14.5	0.97	17.6	13.8	13.7	16.4	12.5	14.8	14.1	14.6	13.7
CaO	23.5	23.6	23.4	20.4	23.5	22.6	22.4	22.7	22.7	23.7	23.5	23.4	23.2
Na_2O	0.25	0.39	0.29	1.17	0.29	0.48	0.83	0.34	0.37	0.29	0.34	0.29	0.30
Total	99.73	100.69	99.25	100.19	99.99	99.41	99.67	99.74	99.35	100.60	100.41	99.70	99.21
Cations based on six oxygens													
Si	1.950	1.793	1.840	1.644	1.953	1.848	1.914	1.925	1.784	1.850	1.831	1.851	1.826
Al	0.062	0.268	0.173	0.682	0.046	0.188	0.104	0.104	0.274	0.163	0.199	0.170	0.199
Ti	0.005	0.029	0.019	0.015	0.005	0.023	0.012	0.006	0.033	0.016	0.017	0.017	0.020
Cr	0.012	0.003	0.012	0.003	0.008	0.003	0.002	0.055	0.001	0.009	0.006	0.008	0.001
Fe^{3+}	0.050	0.114	0.117	0.087	0.048	0.102	0.103	0.091	0.116	0.117	0.124	0.107	0.129
Fe^{2+}	0.055	0.127	0.081	0.541	0.048	0.131	0.149	0.004	0.146	0.081	0.094	0.093	0.110
Mn	0.003	0.005	0.004	0.030	0.005	0.006	0.011	0.004	0.007	0.005	0.006	0.005	0.006
Mg	0.934	0.703	0.802	0.056	0.954	0.763	0.756	0.897	0.700	0.807	0.775	0.803	0.761
Ca	0.918	0.930	0.930	0.853	0.914	0.902	0.890	0.890	0.912	0.931	0.925	0.926	0.927
Na	0.018	0.028	0.021	0.089	0.020	0.035	0.060	0.024	0.027	0.021	0.024	0.021	0.022
DS	3.628	2.885	3.200	1.121	3.670	3.058	3.151	3.447	2.821	3.225	3.104	3.204	3.063
Mg/(Mg + Fe^{2+})	94.4	84.7	90.8	9.4	95.2	85.4	83.6	90.8	82.7	90.9	89.2	89.6	87.4
FeO*	1.81	4.12	2.62	16.57	1.58	4.20	4.78	2.98	4.12	2.64	3.05	3.00	3.52
Fe_2O_3*	1.83	4.11	4.20	2.95	1.76	3.63	3.68	2.01	4.66	4.26	4.47	3.83	4.61

Note: Analysis numbers and labels are keyed to text and figures.
* $FeO = FeO_{tot} - 0.9Fe_2O_3$; Fe^{3+} calculated assuming R_4O_6 stoichiometry and charge balance.
DS = (Si + Cr + Mg + Ca) − (Ti + Al + Fe + Mn + Na).

phenocryst cores. Continuous diffusive re-equilibration between the Fo_{87} core and the outer Fo_{71} surface layer modified the originally steplike compositional profile into the present gradational profile. Mantled xenocrysts and Fo_{71} phenocrysts alike were then plated by more Fe-rich rims subsequent to dike emplacement and consequent rapid cooling.

Phlogopite xenocrysts

The presence of phlogopite crystals in mafic phonolites is an unambiguous indicator of mixing with a minette magma. Biotite did not crystallize until late in the mafic phonolite paragenesis whereas the most distinctive petrographic feature of all the Highwood minettes is the early crystallization of phlogopite. Phlogopite is enriched in MgO, SiO_2, K_2O, and Cr_2O_3 relative to the FeO-, BaO-, and TiO_2-rich composition of the biotite. Analyses 1–6, Table 2, are representative of each of the varieties of mica discussed in the following section.

Phlogopite xenocrysts in mafic phonolites range in shape from rounded to euhedral. All are enclosed by sharply demarcated rims of biotite (Fig. 5). In general, correlations can be drawn among the degree of rounding of the phlogopite cores, the width of the biotite rim, the irregularity of the core-rim boundary, and the mode of emplacement of the mafic phonolite magma. In mafic phonolite crystal tuffs, the euhedral phlogopite xenocrysts have sharply defined, very narrow rims (<2 μm) of bio-

tite. Within dikes of coarser-grained mafic phonolite grading to porphyritic shonkinite, the phlogopite cores may have highly irregular outlines, contain groundmass-filled embayments, and represent only small remnants of larger crystals. Moreover, no phlogopite xenocrysts have been found in coarse-grained, equigranular shonkinites, even in those samples with numerous diopside-cored salite crystals.

Phlogopite xenocrysts rarely occur without accompanying diopside xenocrysts, and diopside occurs as inclusions in some large phlogopite xenocrysts. Several mafic phonolite samples show two populations of phlogopite xenocrysts that are distinguished by their degree of resorption. For these samples, we infer that the less-resorbed phlogopite population was mixed into the mafic phonolite liquid just prior to eruption.

Clinopyroxene xenocrysts

Diopside cores in salite and salite cores in diopside have commonly been attributed to magma mixing in mafic alkalic provinces (e.g., Brooks and Printzlau, 1978; Barton et al., 1982; Pe-Piper, 1984; Duda and Schmincke, 1985). Clinopyroxene occurs in all of the mafic Highwood rocks and shows a compositional range compatible with crystallization from the observed range of magma types (Table 3).

A useful way to discriminate among Highwood province clinopyroxene compositions is to use a cation index

TABLE 3—*Continued*

	Gamma			Delta					Epsilon				Complex	
	14 halo	15 rim	16 micro-pheno	17 salite 1	18 salite 2	19 remnant salite	20 halo	21 residual salite	22 core	23 halo	24 residual salite	25 (111) sector	26 band	27 band
	51.1	43.7	44.4	49.0	48.1	47.2	49.7	51.7	53.7	48.7	51.1	49.9	53.9	51.7
	0.36	1.11	1.23	0.90	1.06	1.17	0.72	0.38	0.20	0.79	0.42	0.73	0.22	0.36
	3.77	8.54	7.44	5.23	5.83	6.75	4.34	3.16	1.10	5.20	3.62	4.24	0.90	2.24
	0.09	0.01	0.05	0.10	0.16	0.04	0.15	0.08	0.34	0.14	0.17	0.18	0.18	0.17
	6.16	13.6	12.2	7.10	8.10	8.31	6.70	5.80	3.67	7.27	6.43	7.07	3.50	6.03
	0.16	0.27	0.24	0.19	0.21	0.20	0.16	0.13	0.13	0.20	0.22	0.23	0.16	0.19
	15.4	8.72	9.69	13.8	12.8	12.6	14.1	15.8	17.1	13.5	15.4	14.2	17.1	15.3
	22.0	22.7	22.8	23.5	23.1	22.9	23.5	22.6	23.8	23.5	22.3	23.4	23.8	23.4
	0.44	0.41	0.40	0.33	0.37	0.43	0.32	0.41	0.29	0.41	0.47	0.35	0.22	0.44
	99.49	99.07	98.41	100.07	99.74	100.15	99.67	100.04	100.43	99.69	100.15	100.26	99.98	99.86
Cations based on six oxygens														
	1.884	1.675	1.705	1.809	1.791	1.757	1.841	1.892	1.951	1.805	1.874	1.836	1.963	1.904
	0.164	0.386	0.337	0.228	0.256	0.296	0.189	0.136	0.047	0.227	0.156	0.184	0.039	0.097
	0.010	0.032	0.036	0.025	0.030	0.033	0.020	0.010	0.005	0.022	0.012	0.020	0.006	0.010
	0.003	0.000	0.002	0.003	0.005	0.001	0.004	0.002	0.010	0.004	0.005	0.005	0.005	0.005
	0.077	0.230	0.211	0.125	0.124	0.153	0.108	0.087	0.047	0.143	0.101	0.122	0.034	0.102
	0.112	0.205	0.181	0.095	0.128	0.106	0.100	0.091	0.926	0.082	0.096	0.095	0.073	0.084
	0.005	0.009	0.008	0.006	0.007	0.006	0.005	0.004	0.004	0.006	0.007	0.007	0.005	0.006
	0.846	0.498	0.555	0.758	0.711	0.700	0.779	0.862	0.926	0.748	0.840	0.781	0.929	0.839
	0.867	0.934	0.937	0.928	0.922	0.916	0.931	0.886	0.927	0.932	0.876	0.923	0.931	0.923
	0.031	0.030	0.030	0.024	0.027	0.031	0.023	0.029	0.020	0.029	0.033	0.025	0.016	0.031
	3.221	2.259	2.439	3.028	2.887	2.784	3.138	3.309	3.640	3.015	3.217	3.123	3.667	3.369
	88.3	70.9	75.4	88.9	84.7	86.8	88.7	90.5	93.5	90.1	89.7	89.1	92.7	90.9
	2.79	7.98	7.30	4.48	4.42	5.46	3.88	3.14	1.71	5.13	3.65	4.41	1.22	3.67
	3.65	6.39	5.64	3.07	4.12	3.40	3.21	2.97	2.13	2.65	3.14	3.10	2.40	2.73

(DS), which is the sum of those cations in which diopside is enriched minus the sum of those cations in which salite is enriched. Therefore, DS = (Si + Cr + Mg + Ca) − (Ti + Al + Fe + Mn + Na), in cation proportions based on six oxygens. The highest DS value measured in diopside is 3.8, and the lowest value measured in salite is 2.8. Plots of DS vs. Al_2O_3, TiO_2, CaO, Mg/(Mg + Fe^{2+}) and Mg/(Mg + Fe_{tot}) for representative pyroxene analyses from a suite of Highwood rocks (excluding analyses of fassaitic crystal rims) show good linear correlations (Fig. 6).

Diopside- and salite-cored pyroxene grains from a large number of samples have been analyzed for this study. These crystals show considerable complexity, and we have selected five representative examples for detailed compositional and textural documentation. From such a treatment we have been able to decipher details of magma-mixing histories that are not otherwise discernible. Two of the examples (Alpha and Gamma) are diopside-cored crystals from the same mafic phonolite sample, and a third (Beta) is from a coarse-grained shonkinite. In addition, two salite crystals (Delta and Epsilon) are described from another mafic phonolite.

Diopside xenocrysts in evolved magmas. Discrete diopside xenocrysts in mafic phonolite represent unambiguous indicators of magma mixing. Diopside cores with salite mantles are more abundant than discrete diopside grains and tend to be more common in rocks containing larger clinopyroxene crystals. Their large size reflects a

protracted growth history affording the opportunity for complex zoning and resorption textures to develop. The following descriptions of Alpha, Beta, and Gamma are presented in order of increasing textural complexity. Alpha is relatively simply zoned but with greater residence time might have evolved to a crystal similar to Beta. Gamma, the most complex diopside-cored xenocryst de-
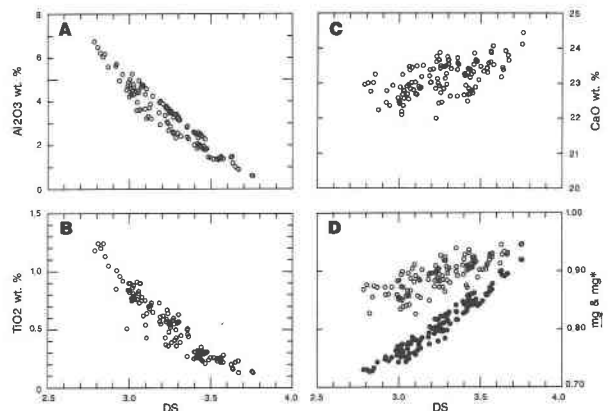

Fig. 6. Variation of Al_2O_3, TiO_2, CaO, mg = Mg/(Mg + Fe_{tot}) (filled circles) and mg* = Mg/(Mg + Fe^{2+}) (open circles) for representative Highwood clinopyroxenes as a function of DS cation index. DS = (Si + Cr + Mg + Ca) − (Ti + Al + Fe + Mn + Na), based on six oxygens per formula unit, and is a measure of the extent of salite substitution relative to diopside.
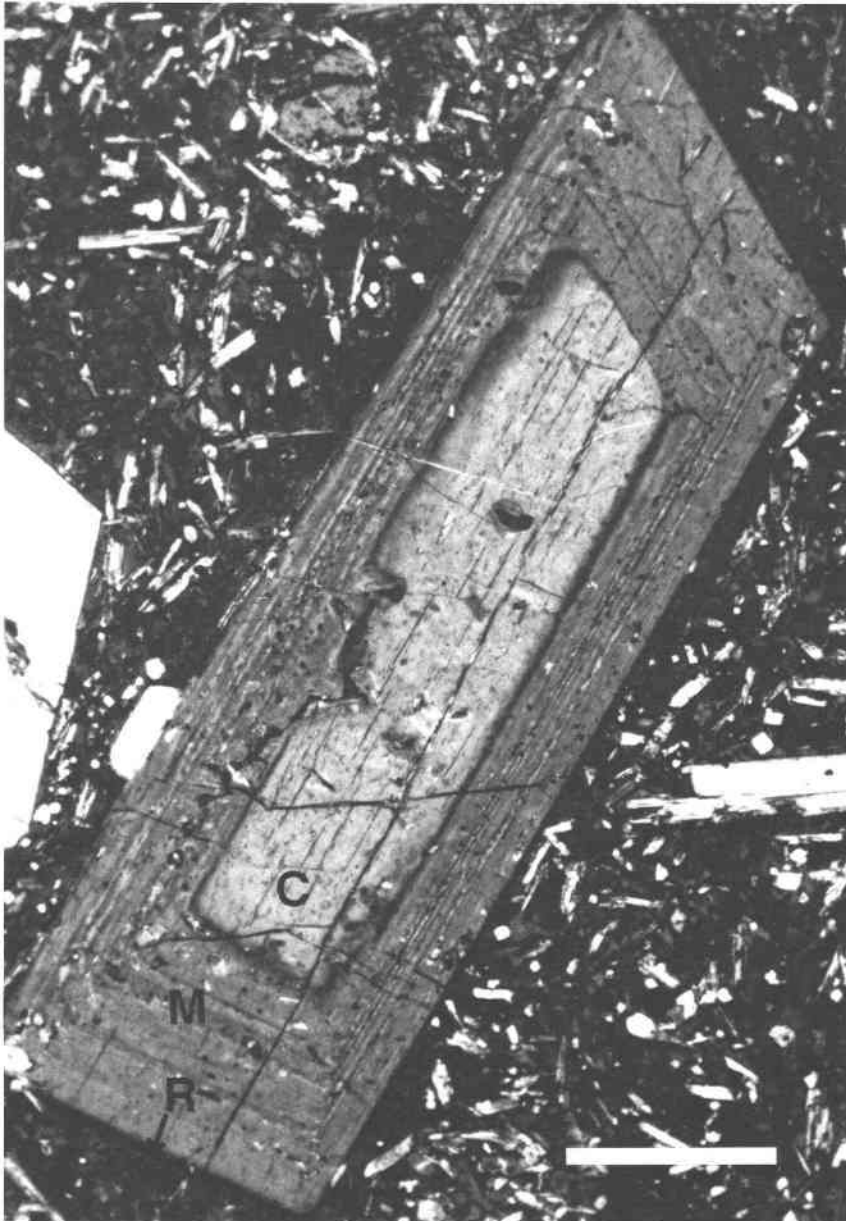
Fig. 7. Clinopyroxene Alpha from mafic phonolite HM-194 (mixed assemblage 4). A rounded and partly corroded diopside core [C] surrounded by a narrow Fe-Al–rich salite band (dark gray) is enclosed by a salite mantle [M] showing sector and oscillatory zoning. A very thin outer fassaitic rim [R] is continuous around the outside of the crystal. Cross-polarized light; scale bar is 0.5 mm.

scribed here, might have developed from a crystal once similar to Beta.

The subhedral, unzoned diopside core (no. 1)[1] of Alpha (Fig. 7) is enclosed in a mantle of sector-zoned salite (no. 3). A band of Fe-Al–rich salite (no. 2) occurs at the contact between the salite mantle and the diopside core. Both the diopside core and the Fe-Al–rich band have rounded

outlines. The outermost fassaitic rim (as low as 1 wt% MgO, no. 4) is continuous around the entire crystal.

The 1 × 3 mm subhedral diopside core (no. 5) of Beta (Fig. 8A) is associated with two different types of salite. The first is a salite mantle similar to that in Alpha. The second occurs as salite halos rimming numerous groundmass-filled cavities within the diopside core. Both the mantle salite and the halo salite contain abundant inclusions of biotite, leucite, titanomagnetite, apatite, and glass. Analyses of this crystal (Fig. 9) show three distinct compositional groups: diopside, higher-Al_2O_3 salite (no. 6),

---

[1] Such numbers refer to a representative point analysis (selected from up to 150 points per grain). The analysis is given in Table 3.

and lower-Al_2O_3 salite (no. 7). The eight most aluminous analyses in the higher-Al_2O_3 salite group (Fig. 9) are from an Fe-Al–rich band in the salite mantle adjacent to the diopside core. This Fe-Al–rich band is discontinuous, and the boundary between it and the outer portion of the salite mantle (lower-Al_2O_3 salite) is spatially irregular yet compositionally abrupt. Halo analyses plot within both salite compositional fields (Fig. 9). The two diopside points that tend toward salite lie within a few micrometers of a salite-diopside contact.

In Gamma, a resorbed diopside core (no. 8) has a salite mantle composed of five distinct compositional bands and an outer fassaitic rim (see sketch, Fig. 8B). These bands are continuous from the [001] zone sector to the ($\bar{1}11$) sector but are much narrower in the former. Traverses from crystal edge to diopside core perpendicular to the *c* crystallographic axis show that Al_2O_3 wt% contents are distinctive for each salite band (see area C, Fig. 8B). Fe-Al–rich band 1 (no. 9), adjacent to the diopside core, and band 2 (no. 10) have rounded outlines and are discontinuous because of the presence of cavities and surrounding halos analogous to those that riddle the diopside core (see area B, Fig. 8B). Salite bands 3–5 (nos. 11–13) and the fassaitic rim do not contain cavities.

Salite halos in the diopside core have Al_2O_3 ranging from 2.9 to 5.6 wt% (no. 14), with widely varying compositions juxtaposed. The most Fe-Al–rich salite in these halos occurs near the diopside-halo contact (see area A, Fig. 8B). A fassaitic pyroxene lines the salite halo-groundmass contacts. This pyroxene is similar in composition to the outer crystal rim (no. 15), the groundmass pyroxenes (no. 16), and euhedral microphenocrysts crystallized within the groundmass-filled cavities.

We infer the following history for the diopside crystals after they were introduced into a mafic phonolite magma: (1) The diopside cores were partly dissolved to produce rounded grains containing a network of irregular cavities. (2) A Fe-Al–rich salite band plated the outside of the resorbed diopside cores and the inside walls of the cavities (compare analyses for nos. 2, 6, and 9, Table 3). (3) The irregular, discontinuous nature and rounded habit of this first salite band implies that this growth layer was also resorbed following further mixing. (4) Multiple, compositionally and optically distinct salite bands in the mantle reflect subsequent episodes of mixing, with each band reflecting a pyroxene grown in equilibrium with succeeding mixed liquids. (5) Fassaitic rims on crystals and interiors of cavities formed during quenching.

The irregularity of the cavity outlines implies that they did not form by trapping of liquid within skeletal crystals. Biotite inclusions of Beta that cross from the salite mantle into salite halos suggest that cavities extended from the diopside edge into the crystal. Moreover, the inner salite-halo boundaries are commonly terminated by euhedral crystal faces, consistent with crystallization into open spaces filled with liquid.

Because inclusions are abundant in the salite mantles and salite halos but are absent from the diopside cores,

the halos could not have formed by the transformation of diopside to salite by a diffusive process. Both salite types must have crystallized from a magma saturated in those phases that occur as inclusions. However, crystals Alpha and Gamma contain abundant leucite inclusions in their mantles, yet occur in a rock devoid of any leucite or leucite pseudomorphs. This implies that they crystallized from a magma different from that which produced the bulk of the rock.

Compositional variations among the salite halos require that several different liquids gained access to the diopside cavities. For example, in Beta, two distinct halo populations exist (Fig. 9). However, for a given crystal, salite halos never show as much Fe-Al enrichment as the first mantle band. For example, Gamma has ~6.3 wt% Al_2O_3 in mantle band 1, whereas the highest Al_2O_3 wt% in the halo salites is 5.6. This may reflect the larger diopside to liquid ratio and greater modification of the salite-saturated liquid within the constricted cavities relative to the outside of the crystal.

Progressive armoring of the cavities by salite may then have restricted further diopside resorption. This possibility is exemplified by the compositional data on Beta (Fig. 9) in that only the first mantle band has compositions distinct from those of the halos. The most compelling evidence that the cavities remained open through the complete crystallization history of these diopside-cored pyroxenes is the nearly identical compositions of the fassaitic pyroxene crystallized both within the cavities and in the liquid surrounding the crystal.

Salite xenocrysts in more primitive magmas. Mixed magmas that are dominated by a minette component (i.e., mixed assemblage 3 in Fig. 3) are not common. The most abundant disequilibrium assemblages that contain resorbed Fe-Al–rich salite are examples of mixed assemblage 5 (i.e., mixing of evolved and more primitive mafic phonolite).

Figure 10A shows a large, zoned, euhedral salite crystal (Delta) with an outer rim that contains numerous groundmass-filled cavities. Delta is normally zoned from salite 1 (no. 17) to salite 2 (no. 18; see sketch, Fig. 10A) and shows both sector and oscillatory zoning. The inner contact of the rim, however, cuts irregularly across this oscillatory zoning and has a patchy zoned texture. Three types of salite exist within this rim: (1) remnant patches of salite 2 (no. 19, see sketch, Fig. 10A), (2) salite halos irregularly surrounding the cavities (no. 20), and (3) more Mg-rich patches between the halos (no. 21). The remnant patches of salite 2 are optically continuous with the crystal core and have very similar compositions (compare no. 18, no. 19, Table 3). Significantly, none of the salite halos of either Delta or Epsilon (see below) contain any of the mineral inclusions abundant in the halos within diopside cores.

Figure 10B shows that this crystal (Epsilon) has undergone preferential dissolution of its [001] zone sector. Epsilon contains a small subhedral diopside core (no. 22) that does not show sector or oscillatory zoning. Outside
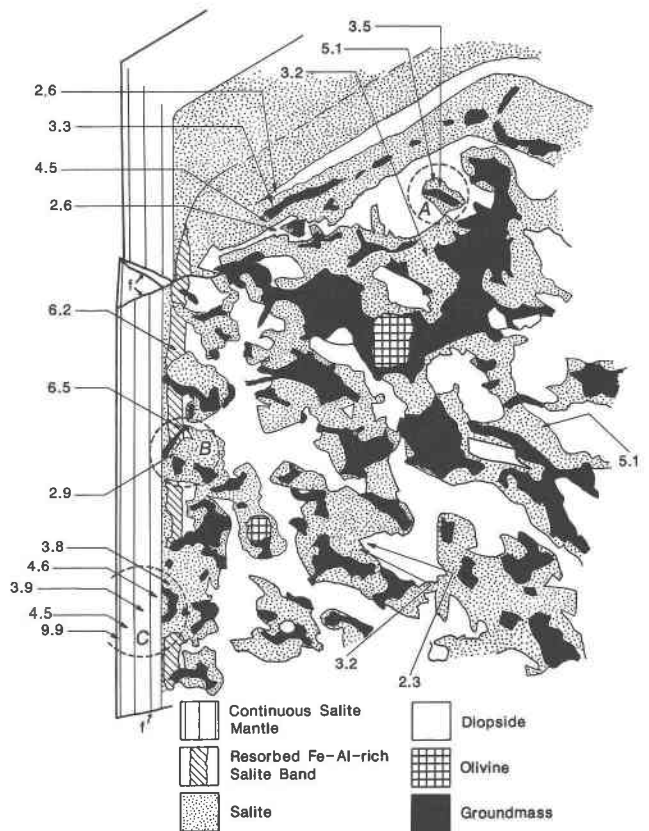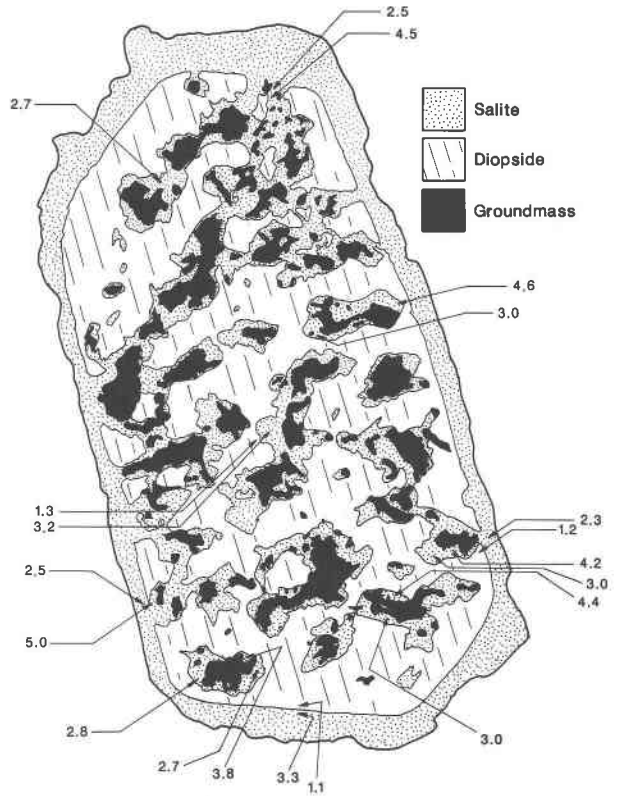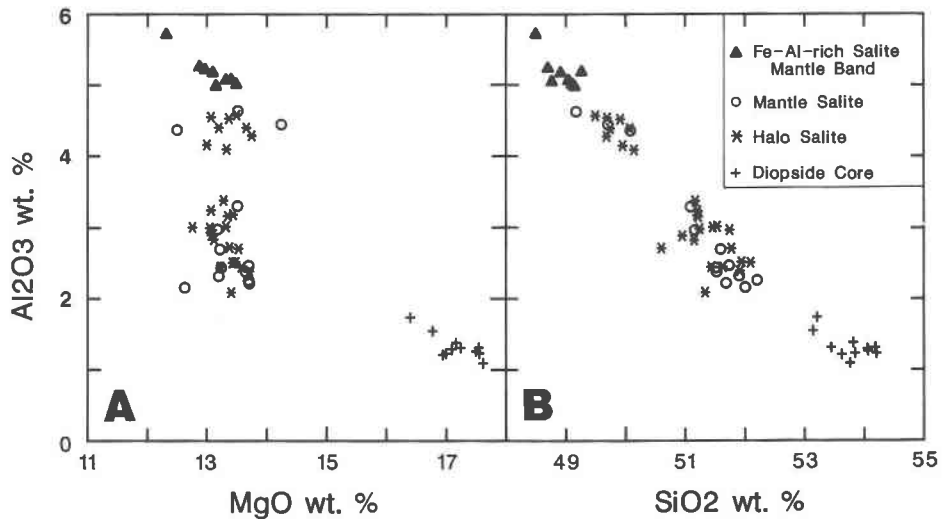
Fig. 9. Variation of Al$_2$O$_3$ with MgO and SiO$_2$ in clinopyroxene Beta, indicating four distinct compositional populations within this crystal. Note the overlap of salite mantle and halo compositions in two of the populations (see text).

of this core, oscillatory zoning is distinct in the ($\bar{1}$11) sector, but the oscillations do not continue into the [001] zone sector. The latter contains numerous groundmass-filled cavities. Relatively uniform salite halos (no. 23) surround these cavities, leaving patches of more Mg-rich salite between halos (no. 24). The unreacted ($\bar{1}$11) sector salite has a composition (no. 25) intermediate between those of the halos and Mg-rich patches. Surrounding and truncating all other zoning is a 1-mm rim of salite equivalent in composition to salite 2 of Delta (see above).

The euhedral habit of the salite xenocrysts (Figs. 10A and 10B) indicates that they reacted by a process different from that affecting the subhedral to rounded diopside cores discussed earlier. Experimental studies of plagioclase dissolution offer insights into these processes. Tsuchiyama (1985a) showed that in the system Ab-An-Di, plagioclase more albitic than that in equilibrium with the starting glass developed mantles composed of micrometer-sized liquid pockets + an anorthite-rich residuum. This partial dissolution continued until the residual crystal reached equilibrium with the liquid. In melting experiments on plagioclase parallelepipeds (Tsuchiyama and Takahashi,

1983), dendritic melting patterns developed with progressive enlargement of the melt pockets until the residual crystal attained equilibrium with the partial melt. Most important for this discussion, a compositional profile developed around each of these melt pockets by the diffusion of albite component toward the melt pockets. The residual crystal remaining between these albite-rich zones was progressively enriched in anorthite.

Textures analogous to those described above in plagioclase occur in salite xenocrysts of the type exemplified by Delta and Epsilon. Assuming that the experiments on plagioclase have relevance for the mixed Highwood magmas, we can infer the following history for these complex pyroxene crystals: (1) Euhedral, oscillatory-, sector-, and normal-zoned salite phenocrysts of an evolved mafic phonolite reacted upon mixing with a more primitive, clinopyroxene-saturated mafic phonolite magma. (2) The entry of relatively Mg-rich, mixed liquid into the outer portions of the crystals produced regions of melt + crystal that obliterated oscillatory and normal zoning, yet left a euhedral crystal outline. (3) Salite component migrated toward the melt-filled cavities, produced diffusion halos,

Fig. 8. (A) Upper two panels. Clinopyroxene Beta from shonkinite HM-215 (mixed assemblage 4). A sieve-textured subhedral diopside core (containing numerous groundmass-filled cavities surrounded by salite halos [H]) is enclosed by a salite mantle [M]. Numbers on the sketch are Al$_2$O$_3$ values (in wt%) from individual microprobe analyses. (B) Lower two panels. Clinopyroxene Gamma from mafic phonolite HM-194 (mixed assemblage 4). A diopside core (containing groundmass-filled cavities surrounded by salite halos) is mantled by five distinct layers of salite and an outer fassaitic rim. Numbers on the sketch are Al$_2$O$_3$ values (in wt%) from individual microprobe analyses; f = fracture; pattern in sketch for mantle salite: band 1 = diagonal rule, band 2 = stippled area between band 1 and unpatterned bands 3–5. Three circled areas illustrate features that are dis-

cussed in the text. Area A: Fe-Al–rich salite halo (5.1 wt% Al$_2$O$_3$) near contact with diopside, which is probably coeval with the innermost salite mantle band 1; remainder of salite in halo has lower Fe and Al contents. Area B: Discontinuity of Fe-Al–rich mantle band 1 with irregular outer boundary (attributed to magmatic corrosion associated with formation of salite band 2) and occurrence of groundmass-filled cavities within salite band 2 that terminate at the inner boundary of the salite band 3 (attributed to corrosion associated with formation of salite band 3). Area C: Continuity and sharp boundaries of salite layers 3–5 and fassaitic rim (indicative of relatively rapid growth and lower degrees of crystal-liquid disequilibrium). Cross-polarized light; scale bar is 0.5 mm.
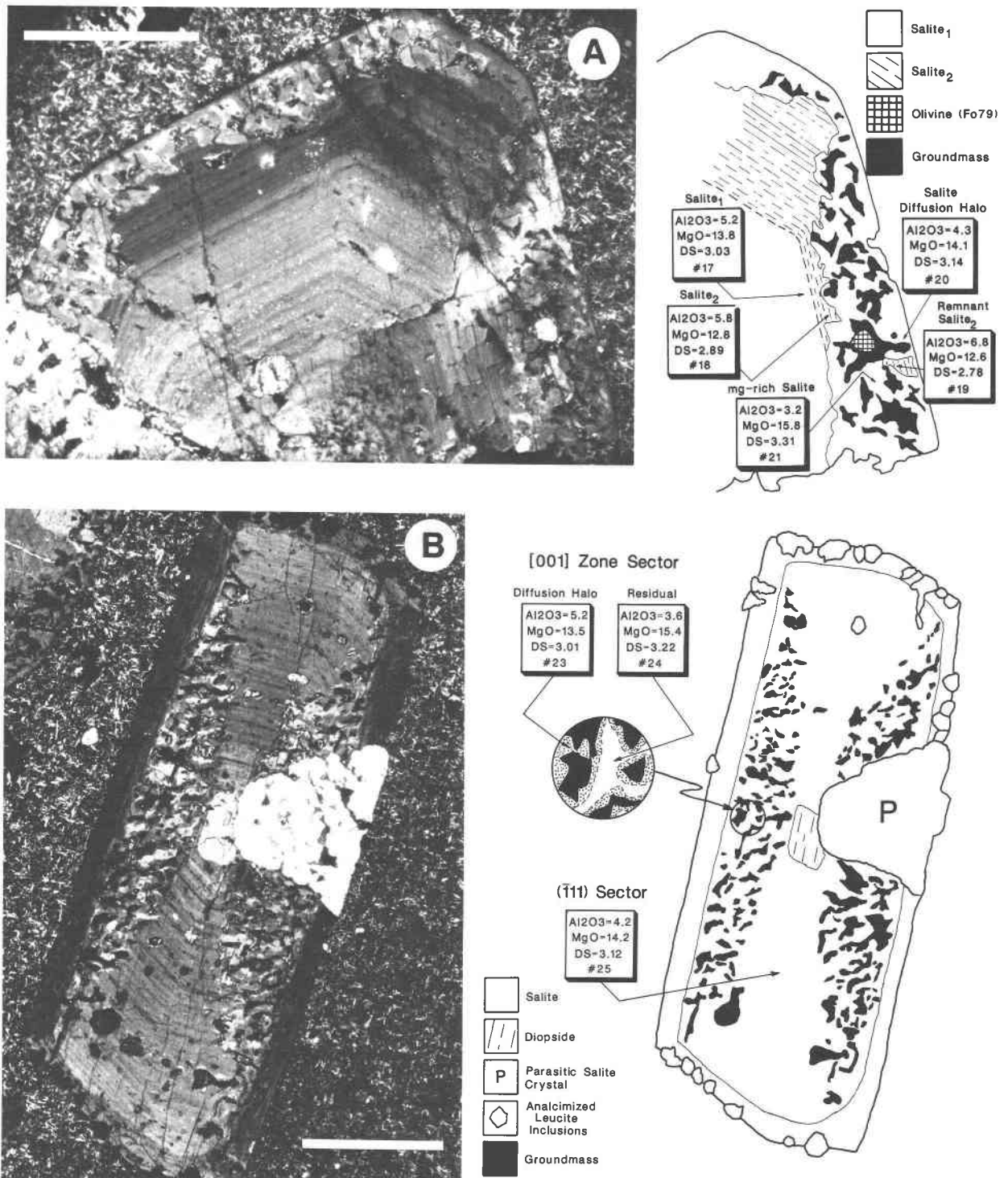
A

Salite$_1$

Salite$_2$

Olivine (Fo79)

Groundmass

Salite$_1$
Al2O3=5.2
MgO=13.8
DS=3.03
#17

Salite
Diffusion Halo
Al2O3=4.3
MgO=14.1
DS=3.14
#20

Salite$_2$
Al2O3=5.8
MgO=12.8
DS=2.89
#18

Remnant
Salite$_2$
Al2O3=6.8
MgO=12.6
DS=2.78
#19

mg-rich Salite
Al2O3=3.2
MgO=15.8
DS=3.31
#21

B

[001] Zone Sector

Diffusion Halo
Al2O3=5.2
MgO=13.5
DS=3.01
#23

Residual
Al2O3=3.6
MgO=15.4
DS=3.22
#24

P

($\bar{1}$11) Sector
Al2O3=4.2
MgO=14.2
DS=3.12
#25

Salite

Diopside

P Parasitic Salite Crystal

Analcimized Leucite Inclusions

Groundmass

Fig. 10. (A) Upper two panels. Clinopyroxene Delta from evolved mafic phonolite HM-13c (mixed assemblage 5). A corroded, xenocrystic salite core (normally zoned from salite 1 to salite 2) has a reacted mantle of more magnesian salite (containing groundmass-filled cavities surrounded by diffusion halos). Olivine within groundmass pockets of the reaction mantle has the same composition as phenocrysts in the sample. Note remnant of salite 2 within reacted mantle. Numbers on sketch refer to complete microprobe analyses given in Table 3. (B) Lower two panels. Clinopyroxene Epsilon from evolved mafic phonolite HM-13c (mixed assemblages 1 and 5). This salite xenocryst (with a small, rounded diopside core) has undergone preferential dissolution of its [001] zone sector. Note the compositional differences between the [001] zone and ($\bar{1}$11) sectors and the Fe-Al enrichment in salite halos around groundmass pockets within the reacted sector (inset). Surrounding this reacted salite is a Fe-Al–rich outer mantle of salite 2 (similar in composition to salite 2 in Delta). Numbers on sketch refer to complete microprobe analyses given in Table 3. Cross-polarized light; scale bar is 0.5 mm.

and left the residual crystal enriched in diopside. (4) Subsequent mixing returned the crystals to an Fe-Al–rich, salite-saturated, evolved mafic phonolite magma that crystallized to form the outer mantle of Epsilon and olivine microphenocrysts within several groundmass-filled cavities of Delta. (5) Fassaitic rims on crystals and interiors of cavities formed during quenching.

In Epsilon, partial dissolution in the [001] zone sector produced cavities surrounded by Fe-Al–enriched diffusion halos that left the residual crystal between the melt inclusions enriched in diopside component (Fig. 10B). Although no primary salite now exists in this sector, we can infer from our studies of sector zoning that it was originally relatively Fe-Al rich compared to the ($\bar{1}$11) sector. The latter was apparently not far enough out of equilibrium to react with the Mg-rich liquid. A simple mass balance shows that the present [100] zone sector (i.e., salite diffusion halos + residual crystal) is approximately equivalent to the ($\bar{1}$11) salite composition. The volume of the melt cavities corresponds to the amount of excess Fe-Al–rich salite component removed.

There are two main lines of evidence that the liquid represented by the present groundmass was less magnesian than the liquid that caused partial dissolution of the salites: (1) As with the cavities described earlier in diopside, the inner surfaces of the cavities in Delta and Epsilon are plated by fassaitic pyroxene similar in composition to microphenocrysts outside of the crystals. Although this Fe-rich fassaitic pyroxene probably represents a quench phase crystallized during rapid cooling after dike emplacement, it does suggest that the last liquid to enter the cavities—and which is now represented by the groundmass of the rock—was not Mg-rich. (2) Olivine phenocrysts in this mafic phonolite range from $Fo_{77.3}$ to $Fo_{79.2}$, and olivine inclusions in cavities of the pyroxenes are Fo_{79}. On the basis of data from experimental studies (e.g., Walker et al., 1979; Sack and Carmichael, 1984), clinopyroxene in equilibrium with Fo_{79} would have Mg/ (Mg + Fe^{2+}) of ~0.82. From the correlation diagrams in Fig. 6, this value corresponds to a DS value of approximately 2.8, which in turn can be used to infer a TiO_2 content of ~1.2 wt% and an Al_2O_3 content of ~6 wt%. The outer salitic pyroxene mantle on Epsilon, which truncates all earlier resorption textures, contains 1.2 wt% TiO_2 and 6.3 wt% Al_2O_3, implying that it is in equilibrium with the olivine phenocrysts and inclusions. The euhedral shape of the olivine phenocrysts implies that they crystallized from the liquid represented by their enclosing groundmass. Therefore, we infer that none of the more Mg-rich salites and diopsides in this sample were in equilibrium with this same liquid and that direct evidence of the more Mg-rich liquid from which these pyroxenes crystallized is now lacking because of mixing processes.

Finally, certain characteristics of Delta (Fig. 10A) can be used to contrast the processes involved in the reaction of diopside and salite subsequent to magma mixing. These include (1) the presence (in the reacted rim) of remnant patches of salite 2 and the absence of analogous diopside patches in mantles around diopside, (2) the absence of inclusions in the salite diffusion halos and their abundance in salite halos within diopside, (3) the euhedral rather than rounded crystal shape, and (4) the less uniform spatial distribution of the salite diffusion halos compared to those in the diopside cores. In summary, partial dissolution of salite xenocrysts formed melt-filled cavities surrounded by *diffusion* halos of salite; whereas the diopside xenocrysts reacted by simple dissolution resulting in cavities that were partly refilled by subsequent salite *crystallization*.

COMPLEXLY ZONED MICA AND CLINOPYROXENE

We use the term "complex zoning" to refer to occurrences of optically and compositionally distinct bands within crystals. These bands have sharp inner and outer boundaries that are, for the most part, parallel to the exterior crystal faces of the host phenocryst.

Clinopyroxene

Complexly zoned salite phenocrysts that contain diopside bands occur in about half of the nearly 300 mafic phonolite and shonkinite samples we have examined (Fig. 11A). However, the distribution of these diopside bands is random in that their occurrence is independent of the salite modal abundance. Those salites with diopside bands show no apparent intercrystal correlations among band distance from the crystal core, band width (10–200 μm), number of bands (up to six but rarely more than four), or the presence of a diopside core.

Compositional profiles. Figures 12A and 12B show compositional variations across two typical salite crystals that contain diopside bands. These profiles show the following features: (1) The diopside band boundaries mark large, abrupt changes in composition over a distance that is typically on the order of 2 μm. (2) The compositions of these bands range from being indistinguishable from those of diopside phenocrysts in minettes and diopside cores in salite to more intermediate, salitic diopside compositions (Table 3, nos. 26 and 27, respectively). (3) Oscillatory zones in the surrounding host salite occur as cyclic, compositional doublets with somewhat consistent amplitudes and recurrence intervals, superimposed on a baseline salite composition (Figs. 12A, 12B). Oscillatory zoning is either subdued or entirely absent from the diopside bands. (4) Salite compositions on either side of diopside bands are commonly different. That is, oscillatory zones are superimposed upon different salite compositional baselines before and after the growth of the diopside band (see Al_2O_3 profile in Fig. 12B).

Band morphology. In general, the wider (~30–200 μm) diopside bands are continuous around the host salite crystal, around crystal clusters (which represent epitaxially grown, radiating crystals that share a common nucleation center), and across all sector boundaries that they intersect (Fig. 11A). These wider bands may, however, contain groundmass-filled cavities analogous to those in the diopside cores described earlier.
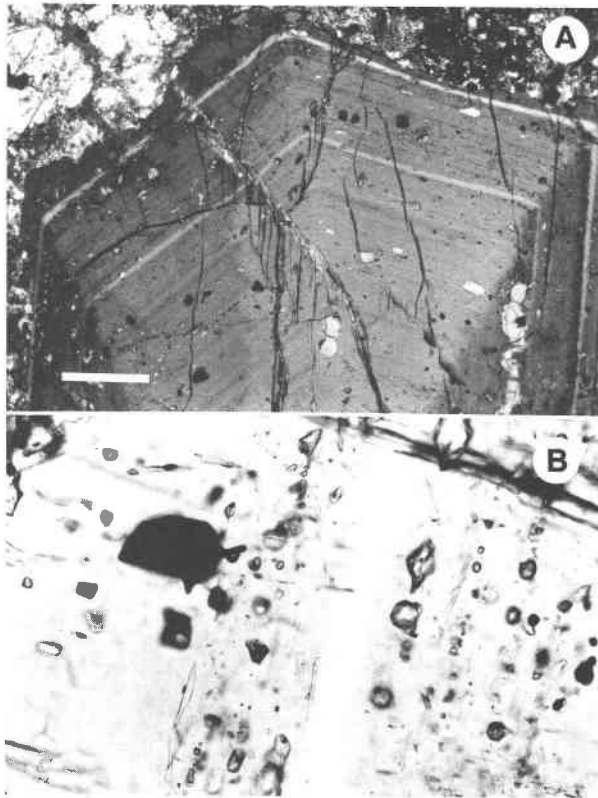
Fig. 11.   (A) Continuous diopside bands (light gray) in a sector-zoned salite crystal from shonkinite HM-220a. The bands record two separate episodes of mixing with minette magma. Cross-polarized light; scale bar is 0.5 mm. (B) Enlarged view of 40-μm-wide diopside band (center, near-vertical) from a crystal in HM-220a. Note absence of inclusions within diopside band and abundance in host salite (apatite, leucite, titanomagnetite, and glass in this view). A microprobe traverse of this band is shown in Fig. 12B. Plane-polarized light.

Fig. 12.   (A) Variation in Al_2O_3 and other oxides across salite crystal from mafic phonolite HM-107. Note the lack of any zoning (normal, reverse, or oscillatory) in the 30-μm-wide diopside band and the prominent oscillatory zoning in the salite. Inset shows variation of four oxides over a larger portion of the same traverse (Incl. = inclusion). (B) Variation in Al_2O_3 across complexly zoned salite crystal from shonkinite HM-220a. Note the lower Al_2O_3 content of salite outside the diopside band in comparison with salite inside the band.

In contrast, the narrower bands (~10–30 μm) may be discontinuous and terminate internally within a [001] zone sector or more commonly at ($\bar{1}$11)-[001] zone sector boundaries (Fig. 13). These truncations produce isolated layers of compositionally and optically distinct pyroxene in the ($\bar{1}$11) sector. Diopside bands may crosscut oscillatory zoning and associated inclusion sheets in those cases where the inner band boundaries are not concordant to the associated external crystal faces. Inner diopside band boundaries may also be irregular even though they remain compositionally sharp (Fig. 13). Irregular outer diopside band boundaries are less common.

Inclusion patterns. The salite phenocrysts are remarkable in the number of ~1–50 μm inclusions of apatite, leucite, titanomagnetite, biotite, and glass they contain. In contrast, the diopside bands are almost entirely devoid of inclusions (see Fig. 11B). Inclusions ~1–10 μm in size in salites tended to nucleate in layers parallel to the crystal faces of the host salite and as such form a distinctive type of zoning. Layers with abundant leucite commonly
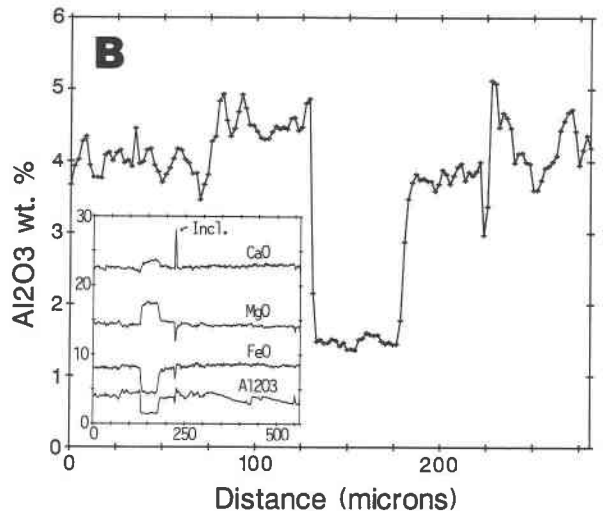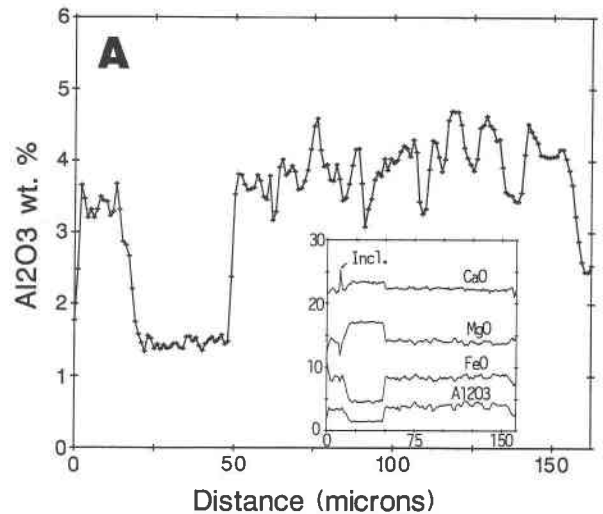
nucleated immediately adjacent to outer diopside band boundaries.

Mica

In samples of mixed assemblage 3, some relatively rare micas with well-developed complex zoning occur (Fig. 14A). Analyses of the phlogopite core and the three surrounding layers from this example are given in Table 2 (analyses 7–10). Except for the outer biotite rim, these growth layers have rounded (resorbed) outlines, yet zon-
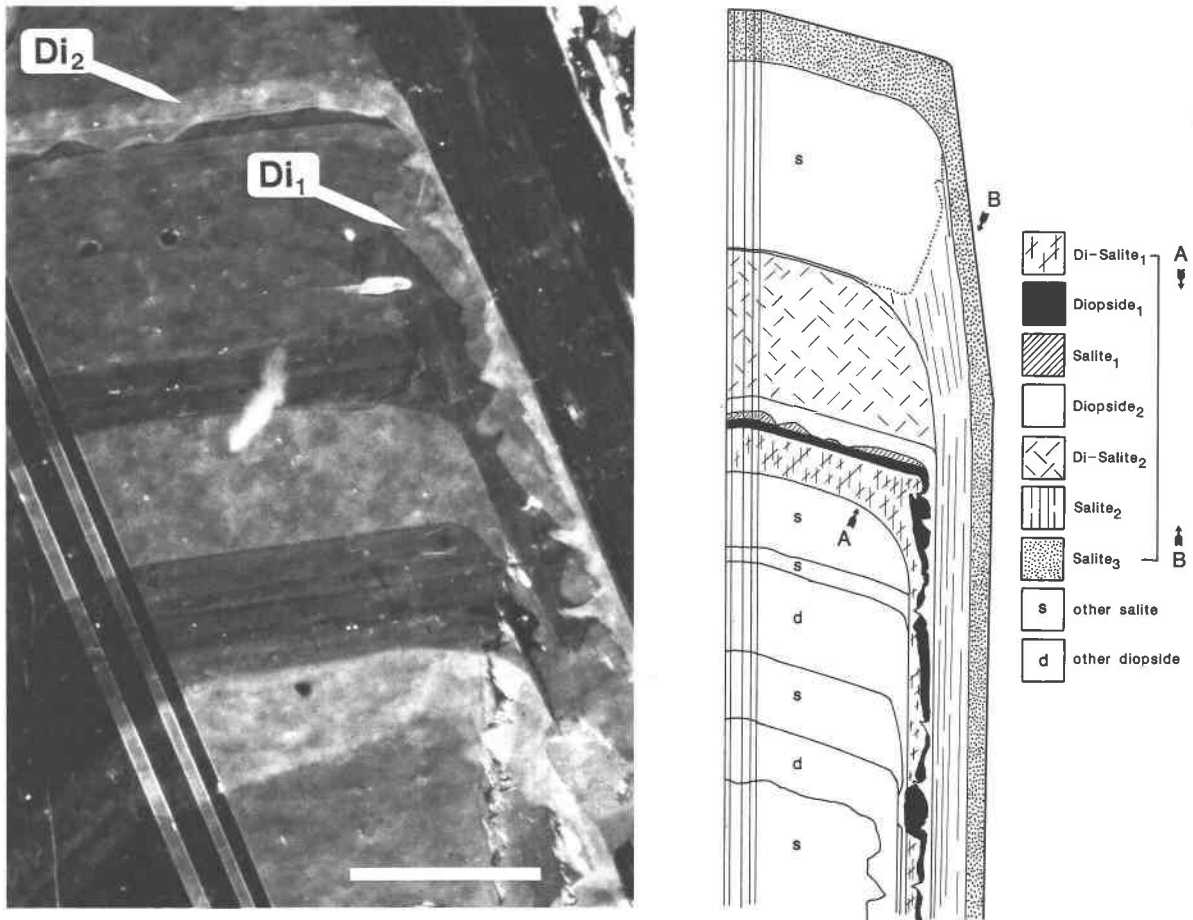
Fig. 13. Clinopyroxene from intermediate minette HM-111 (multiply mixed assemblage 3). This very complex crystal contains multiple separate bands of diopsidic, salitic, and intermediate pyroxene (diopside-salite). Several bands show irregular inner boundaries (see photograph) that are interpreted as evidence of magmatic corrosion prior to successive band overgrowth. In particular, diopside 2 cuts diopside 1 and truncates salite 1, and both diopside bands cut diopside-salite 2. Note prominent oscillatory zoning in the salite and twin planes parallel to c axis. In the sketch the crystal is exaggerated parallel to the c axis to show all compositional layers. Cross-polarized light; scale bar on photograph is 0.15 mm.

ing profiles (Fig. 14B) show that several of these compositional boundaries are sharp. In this example, the inner phlogopite core and the phlogopite band have similar compositions. The intervening Fe-rich phlogopite band has a composition intermediate between that of the phlogopite and the outer biotite rim in all elements except Al (Table 2). More commonly, complex zoning in micas occurs as one single, sharply demarcated phlogopite band within an otherwise compositionally uniform biotite grain.

Phlogopite cores and bands generally cannot be distinguished compositionally from phenocrysts in the minettes and xenocrysts in the mafic phonolites (see Table 2). Likewise, biotite rims developed on these complexly zoned micas have very similar compositions to biotite microphenocrysts from mafic phonolites, biotite plates in shonkinite, and biotite rims developed on phlogopite xenocrysts (Table 2).

Discussion of complexly zoned xenocrysts

Shimizu and le Roex (1986) have described major- and trace-element zoning patterns in augite phenocrysts in alkaline basalts from Gough Island that are analogous to those observed in Highwood pyroxenes. Using ion-microprobe techniques they showed that complementary major- and trace-element variations occur between concentric, sharply bounded augite growth zones. Based on the trace-element variations, they concluded that each of these zones crystallized from a compositionally distinct magma. Diopside bands in salite from other localities have been interpreted as either widely spaced oscillatory zones (e.g., Thompson, 1972, 1977; Downes, 1974; Barton et al., 1982) or have been attributed to magma mixing (e.g., Conrad and Kay, 1984; Morrice and Gill, 1986). Micas with alternating compositional bands have not, to our knowledge, been reported.
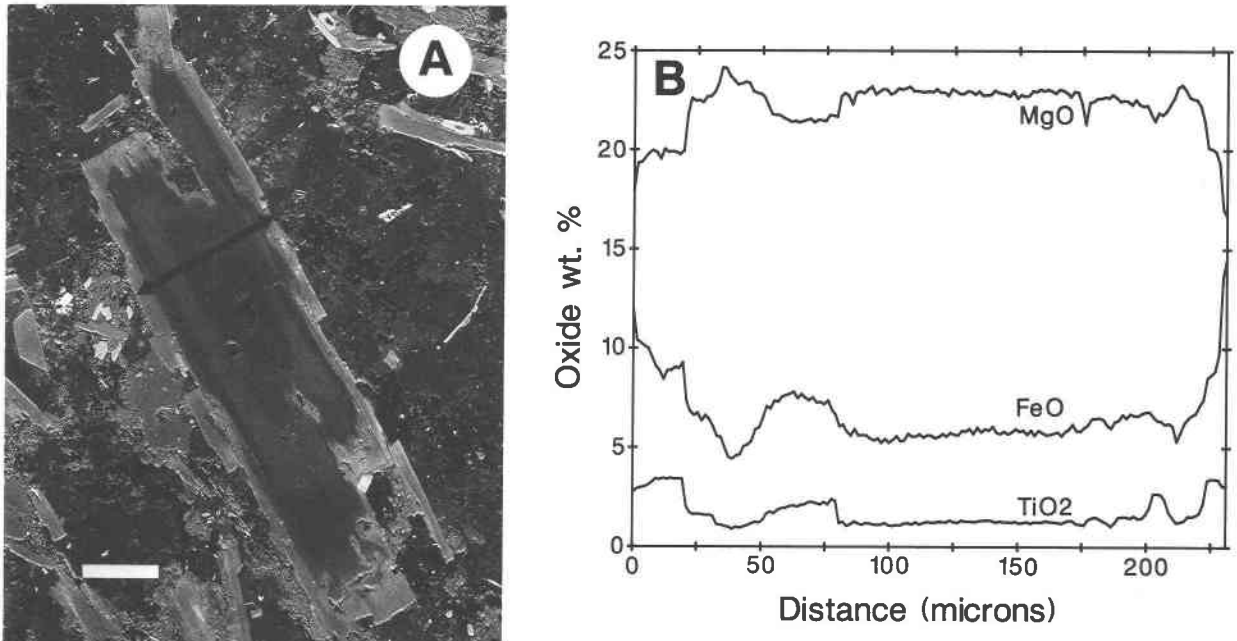
Fig. 14. (A) Complexly zoned mica crystal from mixed mafic phonolite HM-418a (mixed assemblage 3). A xenocrystic core of phlogopite (dark gray) is surrounded by a more Fe-Ti–rich band (medium gray), a phlogopite band, and a biotite rim. This crystal appears to record two separate episodes of growth in a minette-dominated mixed magma. Backscattered-electron image; scale bar is 100 μm. (B) Variation in MgO, total Fe as FeO and TiO_2 along the traverse shown in (A).

On the basis of analysis of a large number of complexly zoned micas and clinopyroxenes from the Highwood province, we have made the following interpretations:

1. Bands representing sharp compositional breaks are developed on euhedral to subhedral crystals. In some of the pyroxene examples, resorbed surfaces truncate oscillatory zoning of the older salite. Resorption, which is not apparently controlled by crystallographic orientation (Kuo and Kirkpatrick, 1985; Tsuchiyama, 1985b), commonly also removed entire compositional bands from [001] zone sectors leaving remnant "beheaded" layers in the ($\bar{1}11$) sector.

2. The randomness of occurrence of bands in complexly zoned crystals implies that several periods of mixing (up to at least six) occurred before final entrainment in the magmas that formed the rocks we have sampled. The fact that some diopside and phlogopite bands in complexly zoned crystals are as magnesian as phenocrysts from the primitive minettes requires that some mixing occurred between these primitive minettes and crystal accumulations derived from mafic phonolites. If mafic phonolite liquids had always dominated the mixtures, then only intermediate composition bands would have formed.

3. Essentially all salite crystals (including phenocrysts and xenocrysts) contain inclusions of apatite, leucite, and titanomagnetite. Inclusions of biotite and olivine are less common. These included phases represent the typical mafic phonolite assemblage and presumably indicate crystallization of the salites from such multisaturated liquids. During diopside crystallization, either the host liquid was not saturated in apatite, leucite, or biotite (i.e., a minette-rich mixed liquid) or the growth of diopside was sufficiently slow to preclude trapping of inclusions (see below).

4. The absence of sector zoning in diopside cores and its occurrence in the host salite and the subdued nature of oscillatory zoning in the diopside bands reflect significant differences in their conditions of crystallization. Rapid crystal growth is known to produce oscillatory zoning (Lofgren, 1974; Downes, 1974) and sector zoning (Wass, 1973; Nakamura, 1973) in crystals.

Observations on zoning and inclusion patterns listed above are consistent with rapid salite growth relative to diopside. Rapid crystallization may have been driven by outgassing of H_2O-rich minette magmas subsequent to and during emplacement at shallow levels within the Highwood magma system (O'Brien et al., 1986). An example of such a process is provided by the large-volume, continuously outgassing 1984 Mauna Loa vent eruption in which the crystallinity of basaltic magma samples increased from 0.5% to 30% over the period of 21 days, yet did so isothermally (Lipman et al., 1985).

IMPLICATIONS FOR THE HIGHWOOD SUBVOLCANIC SYSTEM

The evidence presented here suggests that within the subvolcanic system, mixing between various batches of mafic magmas was the norm rather than the exception. Episodic and repetitive mixing is recognized in the phenocrysts as complexly zoned crystals and resorbed

xenocrysts. Relatively continuous influxes of more primitive mafic phonolite into higher levels of the system may be indicated by the general absence of normal zoning in the salite phenocrysts. This latter feature is apparently not due to high liquid to crystal ratios since no samples with low phenocryst contents have been found.

The diversity in types of mixed assemblages and the heterogeneous distribution of the xenocrysts they contain dictate that one or even just a few large magma chambers underlying the Highwood system would not have been sufficient to produce the diversity that exists. Field evidence showing that the large shonkinite stocks are modally and texturally diverse, on the scale of tens of meters, is consistent with the existence of a large number of small, discrete, transient, magma-filled reservoirs within the subvolcanic system.

The rarity of minette flows in the province, despite the abundance of minette dikes, is a first-order feature requiring explanation. Four of the five volumetrically most important mixing paths (Fig. 3) involve mafic phonolite and minette, yet nearly all of these mixed magmas are dominated by a mafic phonolite component. The occurrences of Mg-rich bands in complexly zoned crystals and Mg-rich cores are consistent with small reservoirs of crystal-rich mafic phonolite being overwhelmed by an influx of primitive minette liquid, followed by remixing into a mafic phonolite–dominated reservoir. The paucity of minette flows can then be attributed to an interconnected system of high-level, relatively outgassed mafic phonolite reservoirs acting as filters through which the primitive minette liquids were rarely able to pass without modification. The fact that the most primitive minettes occur as dikes and chonoliths in the sedimentary sequences surrounding the Highwood core is consistent with this model.

A corollary of this hypothesis is that the minettes probably were parental to the mafic phonolites. The complete compositional overlap between these two mineralogically diverse rock types (O'Brien et al., 1986) implies that they came from similar sources. Degassing of hydrous minette liquids upon arrival in high-level chambers in communication with the surface would have maintained melt composition yet would have resulted in a rapid switch to saturation in an anhydrous phenocryst assemblage (i.e., leucite-phyric). Such a model is consistent with the relative stabilities of phlogopite and leucite in the system kalsilite-forsterite-silica-H_2O as determined experimentally by Luth (1967) and provides for the intimate link between the Highwood minettes and mafic phonolites so apparent in the mixed phenocryst assemblages.

ACKNOWLEDGMENTS

REFERENCES CITED

Barton, M., Varekamp, J.C., and Van Bergen, M.J. (1982) Complex zoning of clinopyroxenes in the lavas of Vulsini, Italy: Evidence for magma mixing? Journal of Volcanology and Geothermal Research, 14, 361–388.

Bence, A.E., and Albee, A.L. (1968) Empirical correction factors for electron microanalysis of silicates and oxides. Journal of Geology, 76, 382–403.

Brooks, C.K., and Printzlau, I. (1978) Magma mixing in mafic alkaline volcanic rocks: The evidence from relict phenocryst phases and other inclusions. Journal of Volcanology and Geothermal Research, 4, 315–331.

Conrad, W.K., and Kay, R.W. (1984) Ultramafic and mafic inclusions from Adak Island: Crystallization history, and implications for the nature of primary magmas and crustal evolution in the Aleutian arc. Journal of Petrology, 25, 88–125.

Downes, M.J. (1974) Sector and oscillatory zoning in calcic augites from Mt. Etna, Sicily. Contributions to Mineralogy and Petrology, 47, 187–196.

Duda, A., and Schmincke, H.-U. (1985) Polybaric differentiation of alkali basaltic magmas: Evidence from green-core clinopyroxenes (Eifel, FRG). Contributions to Mineralogy and Petrology, 91, 340–353.

Dungan, M.A., and Rhodes, J.M. (1978) Residual glass and melt inclusions in basalts from DSDP Legs 45 and 46: Evidence for magma mixing. Contributions to Mineralogy and Petrology, 67, 417–431.

Dungan, M.A., Lindstrom, M.M., McMillan, N.J., Moorbath, S., Hoefs, J., and Haskin, L.A. (1986) Open system magmatic evolution of the Taos Plateau volcanic field, northern New Mexico. 1. The petrology and geochemistry of the Servilleta basalt. Journal of Geophysical Research, 91, 5999–6028.

Fudali, R.F. (1963) Experimental studies bearing on the origin of pseudoleucite and associated problems of alkalic rock systems. Geological Society of America Bulletin, 74, 1101–1126.

Gerlach, D.C., and Grove, T.L. (1982) Petrology of Medicine Lake Highland volcanics: Characterization of endmembers of magma mixing. Contributions to Mineralogy and Petrology, 80, 147–159.

Hearn, B.C., Jr. (1979) Preliminary map of diatremes and alkalic ultramafic intrusions in the Missouri River Breaks and vicinity, north-central Montana. U.S. Geological Survey Open-File Report 79-1128.

Kuo, L.-C., and Kirkpatrick, R.J. (1985) Kinetics of crystal dissolution in the system diopside-forsterite-silica. American Journal of Science, 285, 51–90.

Langmuir, C.H., Vocke, R.D., Jr., Hanson, G.N., and Hart, S.R. (1978) A general mixing equation with applications to Icelandic basalts. Earth and Planetary Science Letters, 38, 380–392.

Larsen, E.S. (1940) The petrographic province of central Montana. Geological Society of America Bulletin, 51, 887–948.

Larsen, E.S., Hurlbut, C.S., Burgess, C.H., and Buie, B.F. (1941) Igneous rocks of the Highwood Mountains, Montana; Part II: The extrusive rocks; Part III: Dikes and related intrusives; Part IV: The stocks; Part V: Contact metamorphism; Part VI: Mineralogy; Part VII: Petrology. Geological Society of America Bulletin, 52, 1733–1868.

Lipman, P.W., Banks, N.G., and Rhodes, J.M. (1985) Degassing-induced crystallization of basaltic magma and effects on lava rheology. Nature, 317, 604–607.

Lofgren, G. (1974) Temperature-induced zoning in synthetic plagioclase feldspar. In W.D. MacKenzie, and J. Zussmann, Eds., The feldspars, p. 362–376. Manchester University Press, Manchester, England.

Luth, W.C. (1967) Studies in the system $KAlSiO_4$-Mg_2SiO_4-SiO_2-H_2O: Part 1, Inferred phase relations and petrologic applications. Journal of Petrology, 8, 372–416.

Marvin, R.F., Hearn, B.C., Jr., Mehnert, H.H., Naeser, C.W., Zartman, R.E., and Lindsey, D.A. (1980) Late Cretaceous–Paleocene–Eocene igneous activity in north-central Montana. Isochron/West, 29, 5–25.

Morrice, M.G., and Gill, J.B. (1986) Spatial patterns in the mineralogy of island arc magma series: Sangihe arc, Indonesia. Journal of Volcanology and Geothermal Research, 29, 311–353.

Nakamura, Y. (1973) Origin of sector-zoning of igneous clinopyroxenes. American Mineralogist, 58, 986–990.

Nicholls, I.A., and Whitford, D.J. (1983) Potassium-rich volcanic rocks of the Muriah complex, Java, Indonesia: Products of multiple magma sources. Journal of Volcanology and Geothermal Research, 18, 337–359.

O'Brien, H.E., Irving, A.J., and McCallum, I.S. (1986) Evolution of minette, lamproite and mafic phonolite magmas in the Highwood Mountains Province, Montana, USA: Geochemical and mineralogical evidence. Extended Abstracts, Fourth International Kimberlite Conference, p. 199–201. Geological Society of Australia, Sydney, Australia.

Pe-Piper, G. (1984) Zoned pyroxenes from shoshonite lavas of Lesbos, Greece: Inferences concerning shoshonite petrogenesis. Journal of Petrology, 25, 453–472.

Pirsson, L.V. (1905) Petrography and geology of the igneous rocks of the Highwood Mountains, Montana. U.S. Geological Survey Bulletin 237.

Raedeke, L.D., and McCallum, I.S. (1984) Investigations in the Stillwater Complex. Part II. Petrology and petrogenesis of the Ultramafic Series. Journal of Petrology, 25, 395–420.

Roux, J., and Hamilton, D.L. (1976) Primary igneous analcite—an experimental study. Journal of Petrology, 17, 244–257.

Sack, R.O., and Carmichael, I.S.E. (1984) $Fe^{2+} \rightleftharpoons Mg^{2+}$ and $TiAl_2 \rightleftharpoons MgSi_2$ exchange reactions between clinopyroxenes and silicate melts. Contributions to Mineralogy and Petrology, 85, 103–115.

Sheraton, J.S., and England, R.N. (1980) Highly potassic mafic dykes from Antarctica. Journal of the Geological Society of Australia, 27, 129–135.

Shimizu, N., and le Roex, A.P. (1986) The chemical zoning of augite phenocrysts in alkaline basalts from Gough Island, South Atlantic. Journal of Volcanology and Geothermal Research, 29, 159–188.

Streckeisen, A. (1979) Classification and nomenclature of volcanic rocks, lamprophyres, carbonatites and melilitic rocks. Geology, 7, 331–335.

Taylor, D., and MacKenzie, W.S. (1975) A contribution to the pseudo-leucite problem. Contributions to Mineralogy and Petrology, 49, 321–333.

Thompson, R.N. (1972) Oscillatory and sector zoning in augite from a Vesuvian lava. Carnegie Institution of Washington Yearbook 71, 463–470.

——— (1977) Primary basalts and magma genesis III. Alban Hills, Roman comagmatic province, central Italy. Contributions to Mineralogy and Petrology, 60, 91–108.

Tsuchiyama, A. (1985a) Dissolution kinetics of plagioclase in the melt of the system diopside-albite-anorthite, and origin of dusty plagioclase in andesites. Contributions to Mineralogy and Petrology, 89, 1–16.

——— (1985b) Partial melting kinetics of plagioclase-diopside pairs. Contributions to Mineralogy and Petrology, 91, 12–23.

Tsuchiyama, A., and Takahashi, E. (1983) Melting kinetics of a plagioclase feldspar. Contributions to Mineralogy and Petrology, 84, 345–354.

Walker, D., Shibata, T., and DeLong, S.E. (1979) Abyssal tholeiites from the Oceanographer Fracture Zone, II. Phase equilibria and mixing. Contributions to Mineralogy and Petrology, 70, 111–125.

Wass, S.Y. (1973) The origin and petrogenetic significance of hour-glass zoning in titaniferous clinopyroxenes. Mineralogical Magazine, 39, 133–144.

Watkinson, D.H. (1973) Pseudoleucite from plutonic alkalic rock–carbonatite complexes. Canadian Mineralogist, 12, 129–134.

Weed, W.H., and Pirsson, L.V. (1895) Highwood Mountains of Montana. Geological Society of America Bulletin, 6, 389–422.

Williams, H. (1936) Pliocene volcanoes of the Navajo-Hopi country. Geological Society of America Bulletin, 47, 111–172.